

The Influence of an Eddy in the Success Rates and Distributions of Passively Advected or Actively Swimming Biological Organisms Crossing the Continental Slope

IRINA I. RYPINA AND LARRY J. PRATT

Woods Hole Oceanographic Institution, Woods Hole, Massachusetts

SAMUEL ENTNER

Raytheon, Waltham, Massachusetts

AMANDA ANDERSON

University of Kansas, Lawrence, Kansas

DEEPAK CHERIAN

National Center for Atmospheric Research, Boulder, Colorado

(Manuscript received 30 August 2019, in final form 18 March 2020)


ABSTRACT

The Lagrangian characteristics of the surface flow field arising when an idealized, anticyclonic, mesoscale, isolated deep-ocean eddy collides with continental slope and shelf topography are explored. In addition to fluid parcel trajectories, we consider the trajectories of biological organisms that are able to navigate and swim, and for which shallow water is a destination. Of particular interest is the movement of organisms initially located in the offshore eddy, the manner in which the eddy influences the ability of the organisms to reach the shelf break, and the spatial and temporal distributions of organisms that do so. For nonswimmers or very slow swimmers, the organisms arrive at the shelf break in distinct pulses, with different pulses occurring at different locations along the shelf break. This phenomenon is closely related to the episodic formation of trailing vortices that are formed after the eddy collides with the continental slope, turns, and travels parallel to the coast. Analysis based on finite-time Lyapunov exponents reveals initial locations of all successful trajectories reaching the shoreline, and provides maps of the transport pathways showing that much of the cross-shelf-break transport occurs in the lee of the eddy as it moves parallel to the shore. The same analysis shows that the onshore transport is interrupted after a trailing vortex detaches. As the swimming speeds are increased, the organisms are influenced less by the eddy and tend to show up en masse and in a single pulse.

1. Introduction

Exchange between the pelagic ocean and relatively shallow continental shelves is a longstanding topic of interest in physical, chemical, and biological oceanography (Brink 1998, 2016; Lentz 2010). Among the various processes and mechanisms that can lead to exchange

is the collision with the continental slope of an impinging mesoscale eddy. This mechanism is relevant to offshore exchange at the edges of the continental shelves of the Mid-Atlantic Bight (Garfield and Evans 1987; Joyce et al. 1992; Ramp et al. 1983; Lentz 2010; Zhang and Gawarkiewicz 2015), the western Gulf of Mexico (Vukovich and Waddell 1991; Frolov et al. 2004), the northwestern Gulf of Alaska (Okkonen et al. 2003), the east Australian shelf (Tranter et al. 1986; Olson 1991), the Antarctic shelf (Stewart and Thompson 2015), and Georges Bank (Lee and Brink 2010). An example that has garnered significant attention involves warm core

 Denotes content that is immediately available upon publication as open access.

 Supplemental information related to this paper is available at the Journals Online website: <https://doi.org/10.1175/JPO-D-19-0209.s1>.

Corresponding author: Irina I. Rypina, irypina@whoi.edu

Publisher's Note: This article was revised on 5 November 2020 to designate it as open access.

DOI: 10.1175/JPO-D-19-0209.1

© 2020 American Meteorological Society. For information regarding reuse of this content and general copyright information, consult the [AMS Copyright Policy](#) (www.ametsoc.org/PUBSReuseLicenses).

rings that are spun off by the Gulf Stream and that propagate westward, toward the continental slope of the northeastern United States. Upon arrival these eddies may strip filaments of water from the continental shelf and/or deposit water on the shelf (Oey and Zhang 2004; Zhang and Gawarkiewicz 2015). Such eddies potentially impact the onshore migration of small organisms such as fish larvae (Hare et al. 2002; Hare and Cowen 1996). Also, cross-shelf transport of fish larvae trapped in eddies spinning off the Florida Current was observed and simulated in Lee et al. (1994) and Limouzy-Paris et al. (1997), and was further linked to episodic settlement of coral reef fishes (Sponaugle et al. 2005).

Slow moving, pelagic organisms may be carried toward the continental shelf if they are caught in a meso-scale eddy that is drifting in that direction, and their trajectories can be further impacted by the complex motion that results when the eddy encounters steep continental slope and the shelf break—the narrow zone of transition to the gently sloping continental shelf. Idealized models of the interaction between an isolated eddy and a shelf/slope topography show that the impinging eddy, upon collision, is partially drained by an along-isobath intrusion, moving in the direction of coastal trapped waves (e.g., Shi and Nof 1993). Primitive equation models with continuous stratification and shelf/slope topography (Oey and Zhang 2004; Wei and Wang 2009; Cherian and Brink 2016, hereafter CB16; Cherian and Brink 2018) show that the intrusion is associated with surface and subsurface secondary vortices and filaments. Observations of intrusions have been documented by Lee and Brink (2010) and Zhang and Gawarkiewicz (2015) in the Mid-Atlantic Bight along with accompanying secondary eddies and filaments. Depending on the location of an organism imbedded in this circulation, the currents may enhance or impede their journey toward the shelf.

The purpose of this work is to identify the detailed cross-shelf transport mechanisms and pathways within the surface flow resulting from an isolated anticyclone colliding with the topography. Specifically, we use a hydrodynamic model with high enough resolution that allows generation of secondary trailing vortices, filaments, and plumes to clarify the extent to which organisms that are initially trapped in an incident eddy are helped or hindered in their journey toward the shelf. We will do so by constructing maps and statistics that show where and when the fluid transport onto the shelf takes place and identify the circulation features responsible for the material and biological transport. Since we are interested in the Lagrangian characteristics of the transport, i.e., tracking material and biological trajectories that cross the shelf break, we rely on Lagrangian

information to construct maps and statistics. In particular, we use finite-time Lyapunov exponents to construct maps that relate the transport pathways to Lagrangian coherent structures, including stable and unstable manifolds. These maps give an indication of the pathways onto the shelf that are relevant for swimming and nonswimming organisms, and they provide a basis for interpreting statistics of arrival times for successful organisms. (For our particular problem, the methods turn out to be most informative in cases of zero or very small swimming speeds.) Attention will be restricted to organisms that swim horizontally at or near the sea surface and that are able to navigate, perhaps using light, water property gradients, or magnetic fields, and can therefore swim directionally.

The fluid velocity fields used for our trajectory calculation are taken from the CB16 numerical simulation of a 3D, anticyclonic eddy that drifts southwestward on a β plane until it encounters a northward-facing continental slope and shelf. The flow far away from the eddy is assumed to be initially quiescent, so we do not consider the influence of preexisting mean circulations such as along-shore currents over the continental shelf. Such circulations are important in applications such as the Mid-Atlantic Bight, where the shelf-break jet is observed to play a significant role in interactions with Gulf Stream Rings (Zhang and Gawarkiewicz 2015). Our study is more generic in that it focuses entirely on the effect of topography. The initial distribution of organisms may be broad or may be confined to the eddy core. In the latter case, we imagine that the organisms have previously been trapped in the eddy core by a process such as detachment from a meandering jet, or simply as the result of the eddy carrying the organisms from one ecosystem to another.

2. Model

The CB16 simulation was carried out using a hydrostatic, primitive equation, β -plane configuration of the Regional Ocean Modeling System (ROMS; Shchepetkin and McWilliams 2005). The model output was saved once daily for 371 days. The numerical domain (Fig. 1) consists of a continental shelf that ranges from 20 to 55 m in depth and is roughly 38.5 km wide, a 50-km-wide continental slope, and a 1225-m-deep offshore region with a horizontal bottom. The shoreline is placed at $y = 0$ and positive y is the offshore direction. The eastern, western and northern boundaries are open to let secondary flow features exit the domain (e.g., westward radiating Rossby waves and along-shelf jets). The domain spans 536 km in the zonal (x) direction with the east, west, and north end boundaries padded by 50-km-wide sponge layers (demarcated by the white lines in Figs. 1, 6, and 8–10). These sponge layers have significantly enhanced lateral tracer

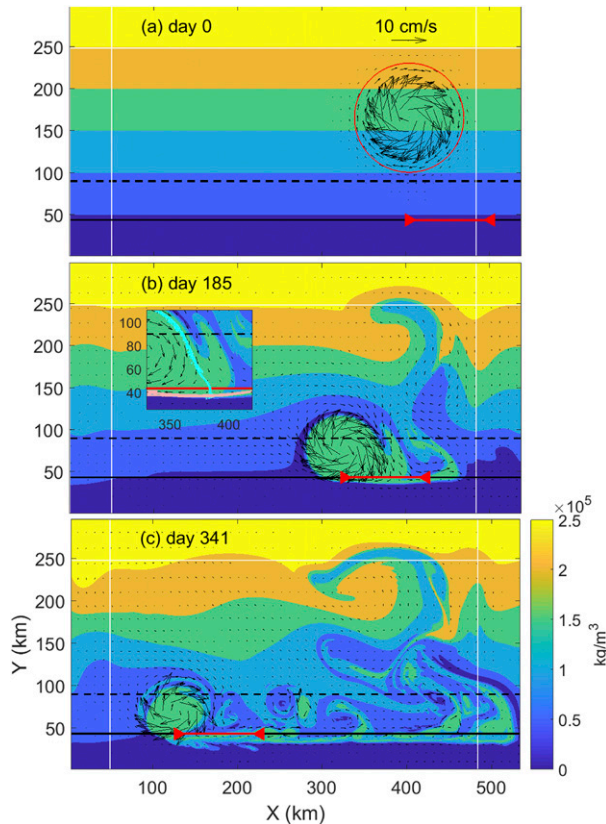


FIG. 1. (a)–(c) Dye concentration for three days with corresponding velocity fields superimposed. White lines represent sponge (high viscosity) regions and black solid and dashed lines at $y = 38.5$ km and $y = 90$ km mark the shelf break and the offshore edge of the shelf, respectively. The red circle in (a) shows the radius used to define our eddy core. The red line marks a segment of the shelf break extending 2 eddy radii to the east from the x position of the instantaneous eddy center. It acts as a moving window through which transport is calculated. The small inset in (b) shows stable/unstable manifolds in cyan/pink in the vicinity of the hyperbolic region just onshore of the shelf break in the lee of the eddy. Manifolds were identified as ridges of the forward/backward-time FTLE fields and correspond to locations with top 85% FTLE values.

and momentum diffusivities that damp boundary-trapped waves as well as noise at the open boundaries. Despite these modifications, small circulations spin up at the western boundary; these are confined to the sponge layer and do not affect the solution in the core of the domain. For computational efficiency the model grid is stretched near each of the open boundaries such that maximum grid spacing is always less than 2.5 km but no less than 1 km. At time $t = 0$ an eddy is initiated with its center located approximately one Rossby radius of deformation (here = 50 km) offshore of deep edge of the continental slope. The eddy is initialized by superimposing an axially symmetric density anomaly on the uniform horizontal background stratification. The density anomaly has a Gaussian distribution in the radial and

vertical directions, with a Gaussian depth scale of 349 m. The azimuthal velocity required to geostrophically balance the pressure perturbation caused by the density anomaly is also imposed as an initial condition and is given at the surface ($z = 0$) by

$$V = (2e)^{1/2} V_o (r/L_o) \text{Exp}[-(r/L_o)^2]. \quad (1)$$

Here r is the radial coordinate, and the maximum velocity V_o (here 0.11 m s^{-1}) lies at $r = L_o/2^{1/2}$, where $L_o = 34$ km. These values are representative of moderate-strength mesoscale ocean eddies. Compared to Gulf Stream rings, which are among the most energetic eddies in the global ocean and reach velocities of 1.2 m s^{-1} at the radius of 45 km (Wei et al. 2008), our simulated eddy is smaller and weaker. Note, however, that due to a smaller Coriolis parameter, $f_{\text{sim}} = 5 \times 10^{-5} \text{ s}^{-1}$, in our simulations compared to $f = 1 \times 10^{-4} \text{ s}^{-1}$ in the Gulf Stream extension region, our eddy is dynamically similar to Gulf Stream rings in terms of Rossby number ($Ro = 0.1$) and also has correct eddy depth to shelf break depth ratio (CB16). In addition to the velocity and density fields produced by the simulation, a passive and weakly diffusive tracer field, initialized with the initial value of latitude y , was computed. Figure 1 shows three select snapshots depicting the evolution of the tracer over the first 342 days of a total integration period of 371 days. Further technical information on the numerical run, including the treatment of the three open boundaries, can be found in CB16 (we use simulation 8341 in their Table 1).

It is well known that an anticyclone on a β plane tends to drift to the southwest (McWilliams and Flierl 1979). This tendency is characteristic of the simulated eddy, though the westward and southward velocity components are not in good quantitative agreement with theoretical predictions for idealized eddies on a β plane (e.g., McWilliams and Flierl 1979). The eddy takes approximately 150 days to reach the shelf break. For organisms that are passively advected, or nearly so, the swirling currents within the eddy and the translation of the eddy as a whole can be crucial to success in reaching the shelf break. The westward and southward components of the translation speed of the eddy center, defined at any instant as the location of minimum surface speed, appear in Fig. 2. There is an initial adjustment period (0–40 days) during which the eddy moves to the southwest, following by a period (40–150 days) in which the dominant motion is southward toward the shelf at approximately $V_e = 0.64 \text{ cm s}^{-1}$. At the end of this period the eddy is positioned over the sloping topography of the shelf and the motion becomes primarily westward, or alongshore, though the speed is erratic. The westward

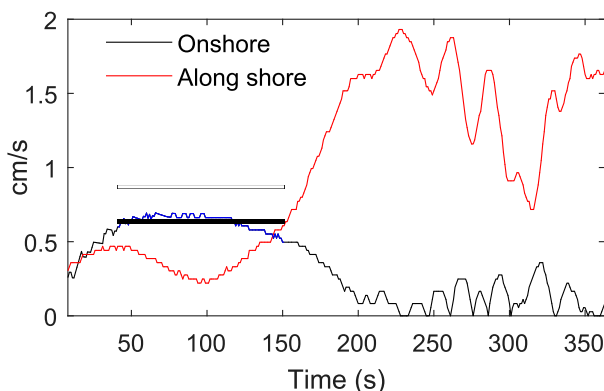


FIG. 2. Onshore and alongshore eddy velocity based on finite differencing the 3-day running time average of eddy center position. Onshore transport during days 40 through 150 is shown in blue. The average onshore velocity over the blue time frame (solid black line) is $V_e \approx 0.64 \text{ cm s}^{-1}$.

direction of propagation parallel to the coast is consistent with the image effect for an anticyclone moving along a wall (Tur and Yanovsky 2017). During the remaining 257 days of the simulation, the westward-propagating eddy leaves behind trailing vortices and a filamented plume of water containing fragments of both the offshore water that has been transported in the eddy core and then expelled behind the eddy, as well as thin streamers of shelf water that get stirred by the eddy and protrude offshore in its wake. (See video SV1 in the supplemental material.) CB16 claim that the interaction between the eddy and the southern wall is qualitatively similar to what happens if the eddy collided with a western boundary with similar topography (see their Fig. 16 for an example).

3. Results

Organisms are considered to have successfully reached the continental shelf if their trajectories cross the shelf break at any time throughout the duration of the simulation. For instance, an organism whose path crosses the shelf break but is then pulled offshore again is still considered to be successful. Additionally, the time at which organisms first cross the shelf is the time recorded for their arrival; subsequent crossing times are disregarded. Experiments are conducted using swimming speeds of $V_s = 0, 0.175, 0.875, 1.75,$ and 8.75 cm s^{-1} or, equivalently, relative speeds of $V_s/V_e = 0, 0.27, 1.37, 2.73,$ and 13.7 with respect to the onshore velocity of the eddy, and $V_s/V_0 = 0, 0.02, 0.08, 0.16,$ and 0.79 with respect to the largest azimuthal velocity of the eddy. These values were selected to illustrate qualitatively different temporal and spatial regimes of arrivals, and were not chosen to match the observed biological behavior for specific species. However, in order to put these numbers in perspective, we note that

observations from laboratory tanks have shown that glass eels—the life stage of American eel after *leptocephali* larvae and before juvenile yellow eel—can swim short term at speeds up to 12 cm s^{-1} (Wuenschel and Able 2008). This estimate is roughly consistent with Tesch et al. (2003) who estimated the overall speed of eel larvae to be 1.4 body length per second; the American eel size at metamorphosis is on average 50 mm (Tesch et al. 2003), giving the swimming speed of 7.5 cm s^{-1} . Note, however, that unlike our simulated organisms, American eel larvae are not surface dwellers and exhibit daily vertical migration between 350 and 550 m in daytime and between 30 and 120 m at night (Tesch 1980; Tesch et al. 1986), so their transport might differ significantly from that of our idealized organisms.

In all cases of nonzero swimming speed (except when explicitly stated otherwise), the simulated organisms attempt to swim directly southward toward the shelf at the indicated speed. Thus the total velocity of the organism is the fluid velocity plus the southward swimming velocity. The ability to swim directionally implies navigational ability, which has not been established for American eel larvae, but which has been identified by Rypina et al. (2014) and Rypina et al. (2016) as a factor that contributes substantially to success in simulations.

Although we are primarily interested in the fate of organisms initially located in the core of the eddy, we also track trajectories initiated broadly over the offshore region. For trajectories initiated within the eddy, we define an eddy interior region consisting of $r < R_0$ with $R_0 = 65 \text{ km}$. This radius corresponds to approximately one e -folding length scale from the maximum velocity V_0 and was specifically chosen to be inclusive, i.e., to encompass all locations with significant azimuthal velocity at $t = 0$. The core region is seeded with 53 078 virtual organisms, with 500-m spacing between neighbors, whose trajectories are followed for the entire duration of numerical model run (371 day). To avoid any uncertainty associated with the stretched grid spacing and spurious circulations in the sponge layers, we restrict the initial positions to the part of the domain where the model grid spacing is 1 km and lateral viscosity and diffusivity are minimal. For organisms seeded over the entire offshore model domain, 469 392 initial positions are distributed randomly offshore of the shelf break with an average grid spacing of 500 m. Trajectories are computed in an offline mode from the saved ROMS velocity outputs using fourth-order variable-step Runge–Kutta integration scheme (“ode45” in MATLAB) with bilinear interpolation in time and space between model grid points. We have made sure that the tolerance value of 10^{-6} used in our integration is sufficient so that the resulting trajectories do not change when tolerance is further decreased.

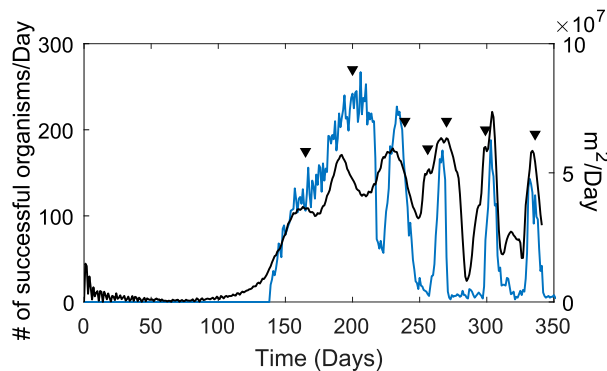


FIG. 3. Time histories of arrivals (blue) for passive organisms and of the surface fluid flux [black, Eq. (2)] across the shelf break within a window trailing the main eddy. The moving window is shown as a red segment in Fig. 1. The arrows show detachment times for trailing vortices, as established by viewing the video SV1.

We first consider the movement of passive non-swimming organisms initially located in the eddy. The blue curve in Fig. 3 gives the time history of successful arrivals (number of successful arrivals per day), with the first arrivals beginning on day 138 and followed by a large group. Beginning around day 210 there is an abrupt dip in rate of arrivals and this is followed by four distinct pulses in arrivals centered near days 230, 264, 300, and 330, and separated by periods of very low arrivals. The pulses are linked to detachment of the trailing vortices seen in Fig. 1 and in video SV1. Detachment times identified by visual inspection of the video are marked by downward pointing arrows in Fig. 3. It can be seen that the four major pulses at the end of the record coincide roughly with detachments. Because the detachment events occur immediately in the lee, i.e., to the east of, the eddy, we next compared the time history of successful crossings to the Eulerian cross-shelf flux in the lee of the eddy. The black curve shows the Eulerian time history of meridional fluid flux $F(t)$ per unit depth (as opposed to Lagrangian particle transport) across a sliding window, aligned in the x direction and positioned over the shelf break ($y_{SB} = 38.5$ km), and extending from the instantaneous x position of the eddy center $x_c(t)$ a short distance ($2L_o$) leeward of the eddy. (This sliding window will be discussed in detail below, but the reader can look back to Fig. 1, where it is shown as a red line segment). Formally the transport across the sliding window segment is given by

$$F(t) = \int_{x_c(t)-2L_o}^{x_c(t)+2L_o} v(x, y_{SB}, t) dx, \quad (2)$$

where v is the meridional component of velocity. Generally, there is a good correspondence between peaks in Eulerian (black) and Lagrangian (blue) transport time series (Fig. 3).

Specifically, the last four major peaks in the Eulerian transport (at around 230, 267, 304, and 335 days) coincide roughly with peaks in Lagrangian particle transport (at around 233, 267, 303, and 332 days), whereas the first two Eulerian peaks (near 165 and 190 days) correspond roughly to the initial ramp-up in the Lagrangian transport (days 140–205). Note also that all the major peaks in both Eulerian and Lagrangian transport time series coincide with the secondary eddy detachment events (indicated by arrows in Fig. 3). Even the secondary peak in Eulerian transport on day 255 (the little bump just before the fourth major peak of the black curve) is proximal to an eddy detachment. We thus observe that intermittency of the time history of both Eulerian cross-shelf transport and Lagrangian particles crossings is closely linked to the trailing vortex detachments.

Since some organisms may be able to swim and navigate, and because organisms may not necessarily originate from the eddy, we now extend the results shown in Fig. 3 to include both complications. In particular, we recomputed the Lagrangian time histories of particle crossings for both passive (Fig. 4 top) and actively swimming (Fig. 4, rows 2–5) organisms, and for both organisms seeded inside the eddy (Fig. 4, left column) and in the much wider domain (Fig. 4, right column). Not surprisingly, as the swimming speed increases, the time history shifts from being dominated by the eddy (as in the passive case scenario in Figs. 4a and 4b) to that dominated by active swimming. Specifically, for organisms seeded in the eddy, the intermittent character of the arrivals, which is linked to the influence of the eddy and detachment events in its wake, remains present in the time series for lower swimming speeds V_s of 0.175 and 0.875 cm s^{-1} (corresponding to about 0.25–1.3 times the onshore eddy propagation speed V_e ; Figs. 4c and 4e), but disappears for the larger values 1.75 and 8.75 cm s^{-1} (Figs. 4g,i). For the latter, the organisms are less dependent upon the ocean circulation to transport them across the shelf break, and the arrival time series are dominated by a single large and increasingly narrow peak (Figs. 4e,g,i), corresponding to a large mass of organisms, all initiated inside the eddy at $t = 0$, that swim directly toward the shelf. This conclusion is supported by comparison of the arrival time histories with the time of arrival of the eddy center (estimated as the initial distance from the shelf break to the eddy center divided by the average onshore eddy propagation speed V_e , red asterisks) with the arrival of the most shoreward row of organisms due to their swimming (estimated as the initial distance from most shoreward organisms to shelf break divided by the swimming speed, black asterisks). As the swimming ability increases, the earliest arrival shifts from the red asterisk to the black asterisk, and the width of the peak in Fig. 4i agrees very well with $\Delta t = 2R_0/V_s$.

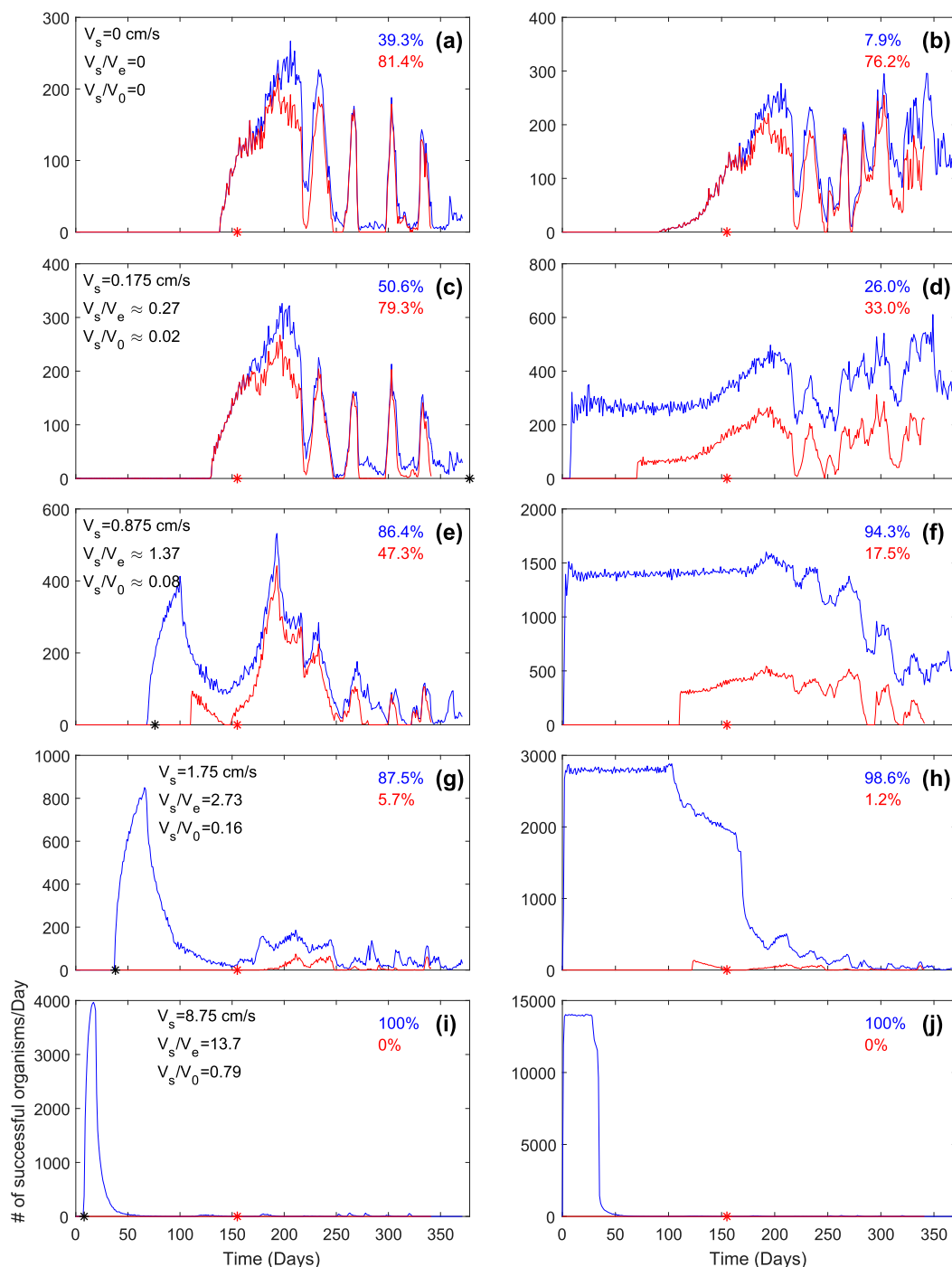


FIG. 4. (a)–(j) Time histories of shelfbreak crossings of organisms for each day (blue curve). Each left/right pair of panels corresponds to a particular swimming speed: $V_s = 0, 0.175, 0.875, 1.75,$ and 8.75 cm s^{-1} from top to bottom; the corresponding ratios of swimming speed to southward eddy translation speed (V_s/V_e) and swimming speed to maximum initial azimuthal eddy velocity (V_s/V_0) are indicated in the left panels. Of the successful organisms, those that meet our criteria for eddy-manifold-induced crossing are plotted in red. The left column shows results for organisms that were initialized within a 65-km radius of the center of the eddy at day zero. The right column applies to organisms initialized in the entire domain off shore of the shelf and to the right of the left sponge layer. The two statistics in each subplot refer to the overall percentage of organisms that succeeded and the subset percentage of those successful organisms that are attributed to the eddy-manifold-induced transport mechanism. For organisms initialized within the 65-km radius, the sample size $N = 53\,094$. For the larger domain outlined above, $N = 469\,392$. The red asterisks are the estimated arrival time of the center of the eddy using V_e . The black asterisks in the left column represent the expected first days of arrival for organisms based on their swimming speed.

The percentage of successful crossings over the entire period is given in the upper right corner of each frame of Fig. 4 and ranges from 39.3% for passively advected organisms to 100% for the highest swimming speed.

The blue curves in the right-hand column of panels in Fig. 4 show the time histories of arrivals for organisms seeded across the much larger region offshore of the shelf break and including those initiated in the eddy but excluding those initiated close to the western sponge region. The episodic character of the time series for nonswimming organisms (Fig. 4b) is still present but lacks the clear separation between episodes of en masse arrivals and those of almost zero arrivals, compared to results for the organisms seeded only inside the eddy. The success rate for all organisms is only 7.9%, much smaller than for organisms seeded only inside the eddy. This suggests that there are very few offshore regions of success apart from the eddy core. When slow swimming is enabled (Figs. 4d,f) we see an immediate, steady pattern of arrivals due to active swimming from organisms that are unaffected by the eddy, followed by intermittency associated with organisms seeded within the eddy core, or within regions of the domain strongly influenced by the eddy. For swimming speeds greater than 1.75 cm s^{-1} , (Figs. 4h,j) the arrival histories are dominated by the initial raft of swimmers and is largely unaffected by the eddy. The success rate is close to 100% in each of the latter two cases.

We now examine the spatial distribution of success and the geometry of the transport pathways across the shelf break. Our primary tool in this study is the finite-time Lyapunov exponent (FTLE) λ , which quantifies the fastest average exponential separation rate between the trajectory of an organism and trajectories of its closest neighbors over an integration time interval T (Haller 2002; Lekien and Ross 2010; Haller 2015). Convenient and fast computation of FTLEs can be accomplished via

$$\lambda(\mathbf{x}_0; t_0, T) = \frac{1}{|T|} \ln \sqrt{\sigma},$$

where σ is the largest eigenvalue of the Cauchy–Green deformation tensor

$$G(\mathbf{x}_0; t_0, T) = (d\mathbf{x}/d\mathbf{x}_0)^T (d\mathbf{x}/d\mathbf{x}_0).$$

Here $d\mathbf{x}$ and $d\mathbf{x}_0$ are the final and initial separations between initially nearby trajectories, computed numerically from dense grids of simulated trajectories. Superscript T denotes the transposed matrix. For a fixed initial time t_0 and integration time T , the result of this calculation provides $\lambda(\mathbf{x}_0; t_0, T)$ —a snapshot of the spatial distribution of forward-time FTLEs at the initial time.

A similar calculation but for trajectories computed backward in time, from t_0 to $t_0 - T$, yields backward-time FTLEs.

FTLEs have been extensively used (not always in a completely rigorous fashion, see Haller 2015) in studies of Lagrangian transport to identify organizing centers of chaotic stirring, specifically, the stable and unstable manifolds of hyperbolic trajectories, in geophysical fluid flows (Rypina et al. 2009, 2010; Ollascoaga et al. 2006; Haller 2015). The stable/unstable manifolds correspond to maximizing ridges of FTLE fields computed in forward/backward time. The underlying reason for the connection between the manifolds and FTLE ridges is that, when present, the stable/unstable manifolds lead to the fast separation of particles initially located on opposite sides of the manifold in forward/backward time, thus producing a ridge in the forward/backward FTLE field extending along the stable/unstable manifold from a hyperbolic trajectory (trajectory that, similar to a hyperbolic stagnation point in steady flows, experiences strong convergence and divergence of nearby fluid in different directions over time). A schematic showing hyperbolic trajectories and their stable and unstable manifolds appears in Fig. 5. In Fig. 5a, the hyperbolic trajectory lies just inshore of the shelf break, with fluid moving away from it along the (red) unstable manifolds, and toward it along the (blue) stable manifolds. Figure 5b shows a situation that will be described later when we consider rapidly swimming organisms. Because velocity shear can also lead to fast particle separation and produce ridges, not all FTLE ridges necessarily correspond to stable/unstable manifolds (Haller 2011, 2015). Additional analysis is generally required to distinguish between shear-dominated and hyperbolic-dominated behavior. However, when the flow is relatively simple so that the existence and general location of a hyperbolic region is transparent from the flow geometry, such as the hyperbolic region located inshore of the shelf break to the east of an eddy (or to the west of an eddy for actively swimming particles) in our flow, maximizing ridges of the FTLE fields that emanate from these hyperbolic regions can be interpreted as proxy manifolds without additional analysis. Note also that in some cases we simply aim to establish a correspondence between locations of successful organisms and ridges of FTLE fields in order to use FTLEs as a diagnostic for regions of success, without making inferences about the type of Lagrangian coherent structures that gave rise to those ridges. One example of a hyperbolic region appears in Fig. 1b, near $x = 380$ and $y = 50$, which lies in the lee (to the east) of the westward propagating eddy and close to the shelf break. Here the onshore (southward) movement of water or organisms associated with the anticyclonic circulation in the eddy

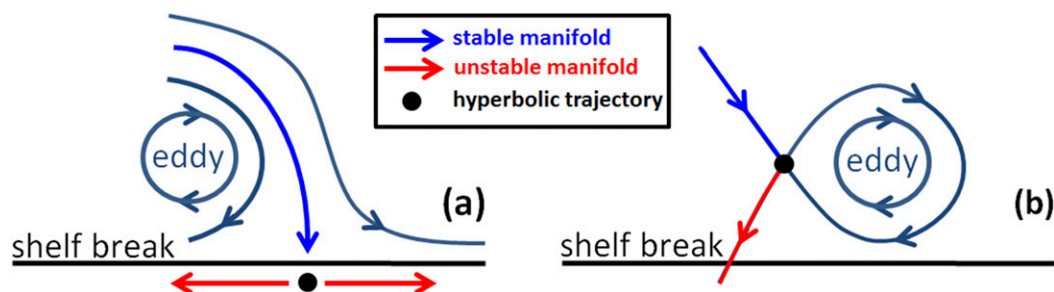


FIG. 5. Schematic diagram showing flow geometry, hyperbolic trajectory, and the associated stable and unstable manifolds for (a) passive organisms and (b) fast-swimming organisms.

splits, with some moving east and some moving west, after crossing the shelf break. The geometry is similar to what is shown in Fig. 5a.

The initial locations of successful organisms for both passive and actively swimming cases are shown by red dots in Fig. 6. The background color shows the 371-day-long forward-time FTLEs. In the passive scenario the majority of successful particles are initially located inside a ring near the perimeter of the eddy, with the minority being distributed in narrow and long filaments closer to the shelf break, to the south and southwest of the eddy (Fig. 6a). The rest of the domain is entirely free of red dots so most passive organisms do not reach the shelf break, consistent with the low success rate estimate ($\sim 7.9\%$) in Fig. 4b. The central core region of the eddy also does not hold any successful organisms; these trajectories simply wind around the center of the moving eddy for the entire duration of the simulation, never crossing the shelf break. In contrast, as illustrated in Fig. 7 and in video SV2, the ring of successful organisms (red ring in Fig. 6 and black ring in Fig. 7) initialized near the eddy perimeter and farther from the eddy center start to leak from the eddy after the eddy approaches the shelf, loses its coherence and starts to shed secondary vortices. The trajectories that start inside the filaments to the southeast of the eddy exhibit very little motion until the eddy approaches their location, at which point they are stirred anticyclonically around the eddy perimeter and deposited onshore behind the eddy. The eastmost filaments, starting with the long “stem” filament extending southward from the eddy, get deposited onshore first, followed by trajectories in the filaments located further west. One important observation forthcoming from Fig. 6a is that the initial locations of all successful nonswimming particles fall on top of the forward-time FTLE ridges (yellow streaks). This is most obvious for the particles in the filaments but is also true for the red ring that is located on top of the tightly coiled and not always well-resolved FTLE ridges. However, the flow also contains FTLE ridges devoid of red dots,

such as the ridges to the northwest or southeast of the eddy; these manifolds do not serve as pathways for cross-shelf transport and are associated with hyperbolic trajectories located offshore of the shelf.

As the swimming speed of the organisms increases (Figs. 6b–e), more trajectories are able to reach the shelf break by active swimming, as opposed to being advected onshore by the currents. For slow swimming speed (0.175 cm s^{-1} , Fig. 6b), only organisms located relatively close to the shelf can make it onshore in 371 days, whereas for the fastest swimming speed (8.75 cm s^{-1} , Fig. 6e) trajectories in the entire domain successfully reach the shelf break over this time. Because of the diminishing role of eddy-mediated, onshore translation and, specifically, disappearance of the hyperbolic regions located on the shelf to the east of the eddy, the agreement between the FTLE ridges, which highlight the pathways (stable manifolds) leading toward the hyperbolic trajectories, and red dots starts to deteriorate with increasing swimming speed (Figs. 6b–d) and is completely lost for fastest swimming speed (Fig. 6e). In the latter case hyperbolic regions no longer occur near the shelf break because nearly all trajectories cross the shelf break, and move onto the shelf and eventually across the shoreline. The connection between locations of successful organisms and maximizing ridges of forward-time FTLEs is lost. Nevertheless, the FTLE fields still provide some useful information about changes in Lagrangian transport with increasing swimming speed. Two notable FTLE features are apparent in a top to bottom comparison of the panels of Fig. 6. First, the low-FTLE eddy core region that was devoid of passive swimmers shrinks to zero with increasing swimming speed—organisms can escape the eddy’s velocity field when they swim fast enough. Second, a strong FTLE ridge is produced to the northwest of the eddy. This feature corresponds to a stable manifold that emanates from a hyperbolic point directly west of the eddy and results from the balance between the offshore eddy velocity and

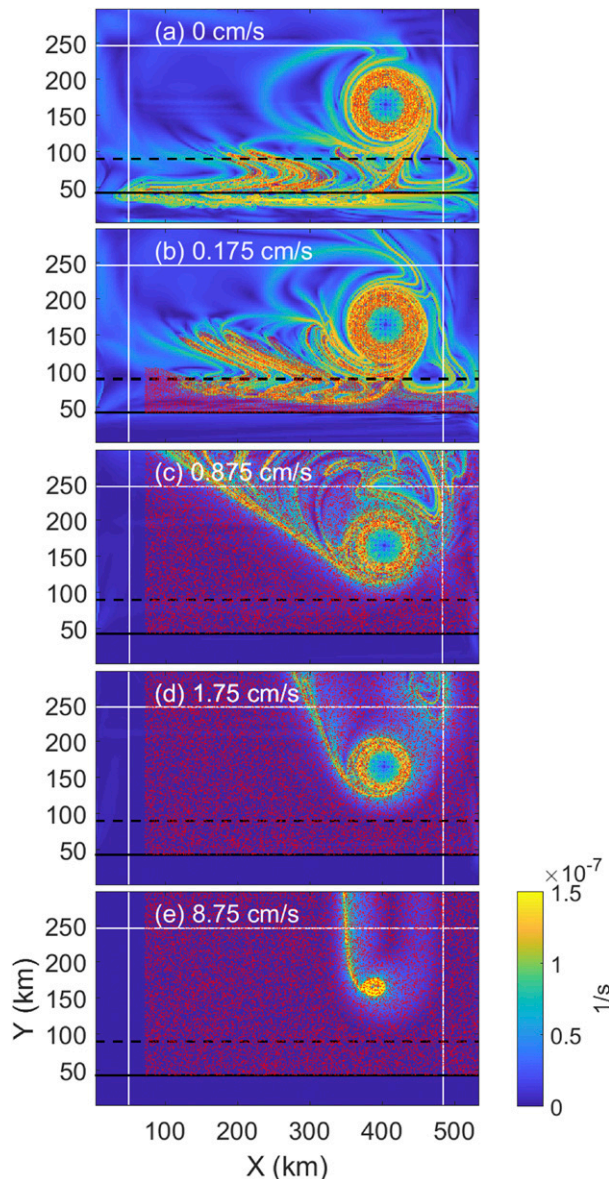


FIG. 6. (a)–(e) Initial positions of a random subset of 20 000 successful organisms (red dots) for different swimming speeds (see Fig. 4 for relative velocity values), overlaid on top of FTLEs (color). For low swimming speeds, successful organisms align well with the FTLE ridges [(a) and (b)]. FTLEs are based on a forward integration from day 0 to 371 and shown on day 0. The horizontal and meridional lines are as in Fig. 1.

onshore swimming velocity at that location (see schematic flow geometry in Fig. 5b). The corresponding hyperbolic trajectory gets shifted closer to the eddy center for faster swimming speeds.

Once the eddy approaches and starts moving westward along the shelf break, a major conduit for the onshore transport of passive particles seems to be the stable manifold emanating from the moving hyperbolic region

located just inshore of the shelf break to the east of the eddy. When evolved forward in time (see Fig. 7 and video SV2), the majority of the red dots from Fig. 6a move onshore along this pathway. The existence of this hyperbolic region is implied by the flow geometry to the east of the eddy (see schematic flow geometry in Fig. 5a). The stable manifold separates inner trajectories that recirculate inside the eddy from the outer trajectories that pass the eddy on the outside and do not recirculate; the former/latter trajectories move westward/eastward past the hyperbolic region. To identify and visualize the evolution of this manifold, we produced daily images of 30-day forward-time FTLEs (video SV2; see also Fig. 8 for three representative images at different stages of the eddy evolution). Because of the shorter integration time used in Fig. 8 compared to Fig. 6, the segments of manifolds revealed by the FTLE ridges are shorter. This is because trajectories located further away along the manifold from the hyperbolic region do not reach the hyperbolic region and thus do not separate from each other over 30 days. At day 0, no FTLE ridges are visible in Fig. 8a because no significant separation between particles occurs from day 0 to 30. When the eddy approaches the shelf, a prominent FTLE ridge corresponding to the stable manifold described above forms in the lee of the eddy. The hyperbolic trajectory that acts as an attractor for this ridge, depicted as a black dot in Fig. 5a, lies near $x = 375$ and $y = 48$ in Fig. 8b. As time progresses, these features are disrupted by the detachment of trailing vortices and the manifolds become increasingly tangled (e.g., Fig. 8c), but a prominent stable manifold reemerges after each such event. In Fig. 8c, where the eddy has moved a substantial distance westward along the shelf break, a bright yellow stable manifold and terminating hyperbolic trajectory can be seen near $x = 145$, $y = 48$.

The changes in the 30-day forward FTLEs with swimming speed are presented in Fig. 9, which shows FTLE snapshots at day 185 for the same five values of swimming speed as in Fig. 6. As anticipated from Figs. 6 and 8, the geometry of the FTLE ridges shifts from that dominated by the above-described manifold behind the eddy (which serves as a major cross-shelf pathway for passive organisms; see Fig. 5a) to that dominated by the manifold in front of the eddy, which emanates from the hyperbolic trajectory at which fluid velocity is equal and opposite in sign to the swimming velocity (see Fig. 5b). Associated with this hyperbolic trajectory, in addition to the stable manifold, which corresponds to the maximizing yellow ridge in forward-time FTLEs that extends to the northwest from the eddy in Fig. 9e, there is also an unstable manifold that can be identified as a maximizing ridge of the backward-time (rather than forward-time) FTLEs.

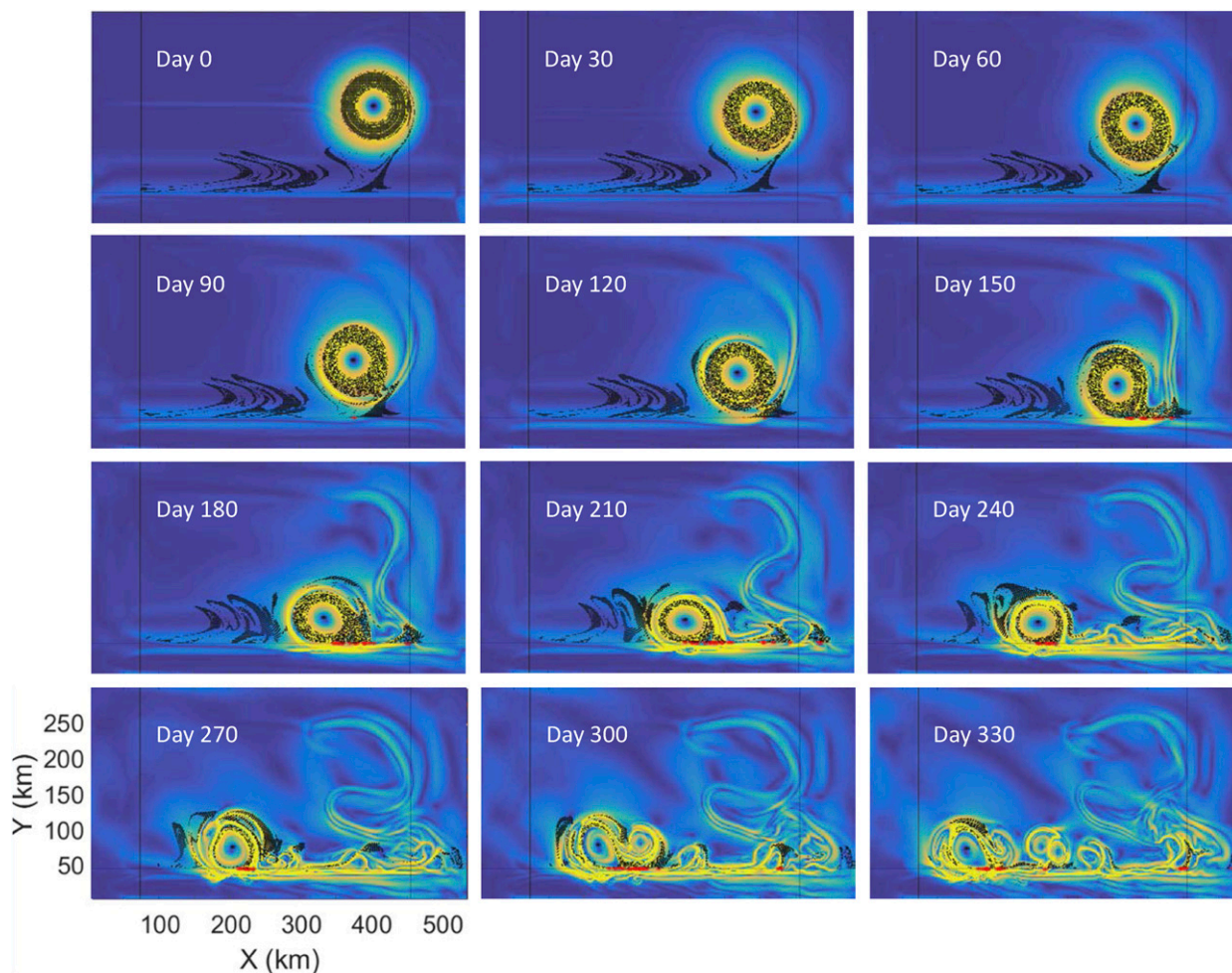


FIG. 7. Locations of all successful passive organisms (black dots; same as red dots in Fig. 6a) every 30 days. Locations of those organisms that cross the shelf break on a particular day are in red. Background color corresponds to 30-day forward FTLEs (same as in Fig. 8).

The geometry of Lagrangian motion for fast swimmers, which is schematically illustrated in Fig. 5b, with the hyperbolic region just west of the eddy and the stable/unstable manifolds emanating from it away/toward the shelf, was further confirmed in Fig. 10, which shows a superposition of the forward- and backward-time 30-day FTLEs on day 48. We remind the reader that (with some caveats) maximizing ridges of the forward-/backward-FTLEs are proxies for stable/unstable manifolds. Because of the absolute value of integration time T in the denominator in the definition of FTLEs, both forward- and backward-time FTLEs are positive, so to distinguish between forward- and backward-FTLEs, we show the difference, $\text{FTLE}_{\text{backward}} - \text{FTLE}_{\text{forward}}$ in Fig. 10 (rather than the sum, in which case the blue streak would have been yellow). The stable/unstable manifold in this figure corresponds to the blue/yellow ridge extending northeast/southwest from the eddy. The

unstable manifold is densely populated by the red dots, which show instantaneous locations of successful fast-swimming organisms still remaining offshore of the shelf break on that day. Note, that by day 48 most of the successful fast swimmers have already crossed the shelf, in agreement with Figs. 4i and 4j that show a sharp drop-off from in the number of arriving organisms around day 40. Thus, red dots in Fig. 10 identify “stragglers,” i.e., organisms that started well offshore and were slowed in their arrival at the shelf break as a result of interaction with the eddy. For these straggling fast-swimming organisms, it is this unstable manifold to the west of the eddy (rather than the stable manifold to the east of the eddy as in the passive advection case) that provides the dominant onshore pathway (see also video SV3). All of the stragglers eventually reach the shelf by the end of simulation (as evident from video SV3), in full agreement with Fig. 6e, which shows that all organisms have arrived at the shelf by day 371.

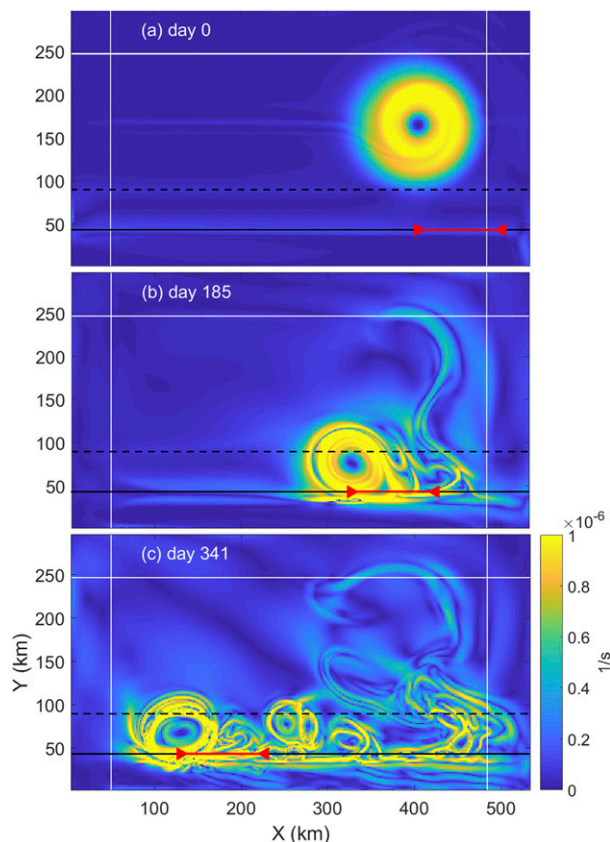


FIG. 8. 30-day forward FTLE images for passive organisms. Red marks the segment of the shelf break extending 2 eddy radii to the east from the x position of the instantaneous eddy center. The horizontal and meridional lines are as in Fig. 1. The time in each image also corresponds to the times in Fig. 1.

We now turn our attention back to the Lagrangian geometry of motion for the passive and slow-swimming organisms. In this case, we have suggested that the presence of the stable manifold in the immediate lee of the eddy, and the associated onshore advection, are closely associated with successful shelf break crossings. We can quantify the importance of this link by computing the number of successful crossings that take place in the lee of the eddy when a stable manifold is present. To qualify, a crossing must occur within two eddy radii to the east of the instantaneous x position of the eddy center, as indicated by the red segment in Figs. 1, 8, and 9, and must do so when a maximizing ridge of the 30-day forward FTLE field is present within that segment. Events satisfying both conditions are referred to as “eddy-manifold” crossings. As an example, an organism crossing the red segment of the shelf break in Fig. 8a or Figs. 9d and 9e would not be considered eddy-manifold-induced because there was no FTLE ridge crossing the red segment of the shelf break at that time. The time

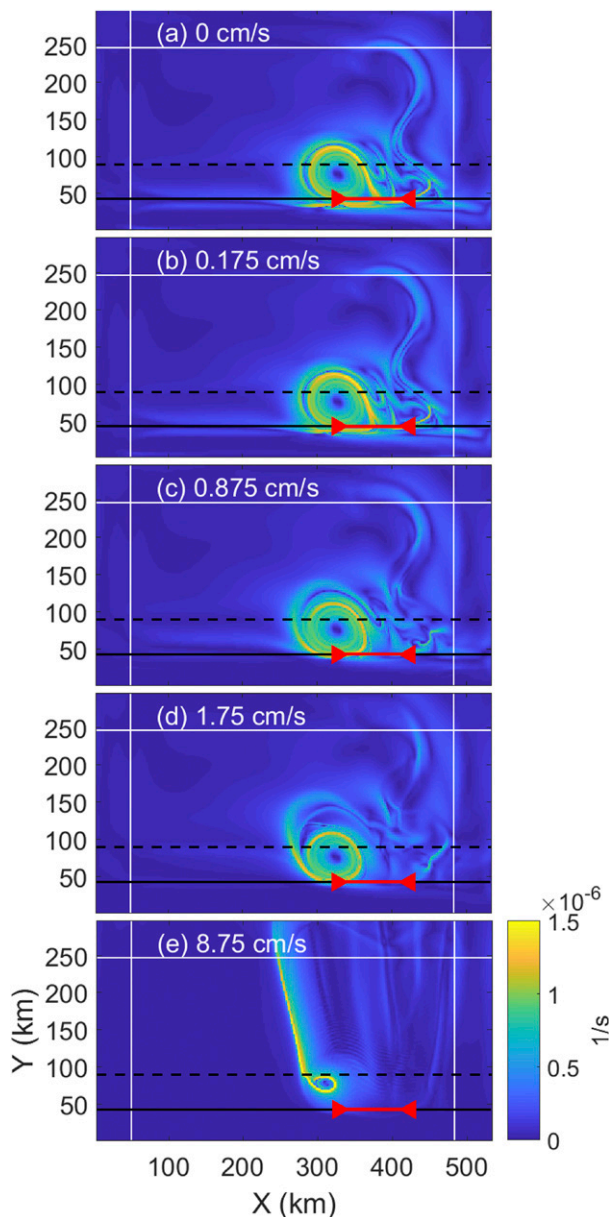


FIG. 9. 30-day forward FTLEs on day 185 for different swimming speeds (see Fig. 4 for relative velocity values). Red marks the segment of the shelf break extending 2 eddy radii to the east from the x position of the instantaneous eddy center with the manifold region in red. The horizontal and meridional lines are as in Fig. 1.

histories of the eddy-manifold-induced crossings are shown in red in Fig. 4, with the red number in the top right corner of each panel quantifying the percentage of total crossings that were attributed to the eddy-manifold-induced cross-shelf transport mechanism. For passive organisms (Figs. 4a,b), the red curve matches closely with the blue curve, so the percentage of the eddy-manifold-induced crossings is very high (>75%). This confirms that for passive organisms, the stable

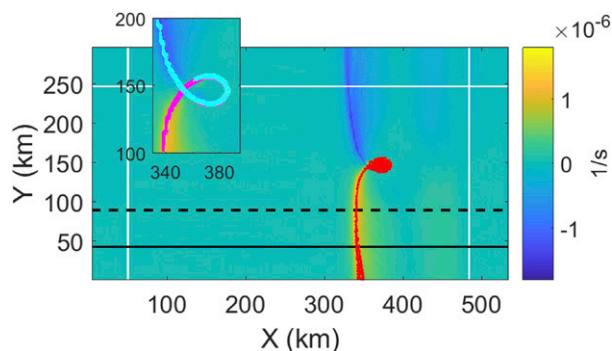


FIG. 10. Superposition of forward (blue to green) and backward (green to yellow) 30-day integration FTLEs for organisms swimming at 8.75 cm s^{-1} on day 48. Red dots represent the positions of every fifth successful organism on this day. The horizontal and meridional lines are as in Fig. 1. Small inset shows the stable (unstable) manifolds in cyan (magenta) colors, identified as the maximizing ridges (locations with 90% largest values) of the forward-/backward-time FTLE fields.

manifold to the east of the eddy serves as the major onshore pathway. For actively swimming particles, the manifold still contributes to depositing organisms onshore, but its importance decreases rapidly with swimming speed (from 79.3% in Fig. 4c to only 1.2% in Fig. 4h). The percentage of the eddy-manifold-induced crossings decreases to 0% for a swimming speed of 8.75 cm s^{-1} , confirming that fast swimming organisms are not significantly influenced by the eddy and its associated flow structures.

4. Discussion and summary

Our investigation fits into the broader topic of transport of biological organisms from the deep ocean to a shallow continental shelf. We focus specifically on the collision between an isolated, mesoscale, anticyclonic eddy and idealized slope/shelf geometry and how the resulting fluid motion affects the success and distribution of organisms that are attempting to reach the continental shelf from offshore. We consider passive (nonswimming) organisms and also organisms that can swim and can navigate directly toward the shelf. Our model is quite idealized in many respects, some related to the limitations of our oceanographic model, whereas others are related to the assumed swimming and navigation of organisms. Specifically, we use simplistic bathymetry and assume that all fluid motion is due to a single, isolated eddy. Motions due to the wind or meandering shelf break jets or other alongshore flows may be important in specific applications but are disregarded here. Tides are also not included, and we use daily (rather than more frequent) model output, which can influence the arrival of organisms from the deep ocean onto

the shelf. On the biological side, we confine attention to organisms that remain at or near the surface (i.e., topmost grid cell), whereas in reality only 1% of *leptocephali* larvae are found at the sea surface; they typically dwell down to a few hundreds of meters (Richardson and Cowen 2004; Tesch et al. 1986) and/or often undergo daily vertical migration. Our organisms are also either passive or swim directly toward shelf at a constant speed, even though real larvae might adjust their speed and/or direction. Nevertheless, we hope that our idealized study will help build a foundation for future, more realistic biophysical studies of larval transport specific to certain biological species.

The simulated eddy has a radius of approximately 30 km at the location of a peak azimuthal velocity of about 10 cm s^{-1} , both of which are typical of mesoscale ocean motions of moderate strength. The eddy is dimensionally smaller and weaker than many Gulf Stream warm rings but is nondimensionally quite similar to those rings in terms of Rossby number and ratio of eddy depth to shelf break depth (Cherian and Brink 2016). For passive (nonswimming) organisms initially distributed over the eddy interior, we identify a subset that will successfully cross the shelf break within the 371-day simulation time. This subset is mostly distributed over a ring that occupies the outer part of the eddy. Inside of this ring is a core of fluid that remains trapped within the eddy throughout the simulation time and never reaches the continental shelf. As the eddy approaches the shelf break and then turns and moves parallel to the shelf break, the eddy advects fluid from the ring across the shelf break. This transport occurs in the lee (to the east) of the eddy, where the circulation of the anticyclone is predominantly onshore. Additional filaments or distinct thin streaks of organisms, which are initially distant from the eddy and not located in the above-described ring, are also carried inshore and across the shelf break as a result of this motion; these organisms stay virtually motionless until the eddy approaches them along the shelf break from the east, at which point they get entrained into the anticyclonic motion and get deposited to the shelf east of the eddy. The deposition of fluid on the shelf is interrupted by the intermittent detachment of secondary eddies in the lee of the primary anticyclone. The onshore transport therefore occurs in pulses, with different groups of trajectories brought across the shelf break at different locations. Fluid that has crossed the shelf break typically turns and flows parallel to the coast (and sometimes leaves the shelf later on), and does not experience substantial inshore penetration further across the shelf. These fluid parcels form an alongshore current of cross-shelf extent one Rossby deformation radius propagating downstream in the coastal-trapped wave direction (e.g., Cherian and Brink 2018; Zhang and Gawarkiewicz 2015). Some degree of acquired

swimming ability appears to be necessary for the organisms to cross the shelf and reach the shore.

The scenario described above is supported by analysis of the forward FTLE fields, which provide a map showing transport pathways. Successful nonswimming trajectories always lie on top of proxy stable manifolds corresponding to maximizing ridges of the forward FTLE plots. The correspondence between stable manifolds and on shore transport can be attributed to the fact that the onshore flow in the lee of the eddy tends to split as it crosses the shelf break, some turning east and some west, thereby giving rise to a hyperbolic region. A ridge of high FTLE values corresponding to a proxy stable manifold extends from this region in the offshore direction. This manifold acts as transport pathway for the onshore flow.

When the organisms are given the ability to swim toward shore at a constant velocity, the influence of the eddy remains significant provided that the swimming speed is less than about 1 cm s^{-1} ($V_s/V_e = 1.6$; $V_s/V_0 = 0.1$). The arrivals still occur in pulses and much of the transport across the shelf break occurs in the lee to the east of the eddy. However, these features become less predominant as the swimming speed is increased, in our case from 0.875 to 8.75 cm s^{-1} . For the latter the majority of organisms cross the shelf break in a large single pulse, the timing of which is largely dictated by swimming speed and initial location, and not advection by the eddy. When the swimming speed reaches the largest value considered (8.75 cm s^{-1}) virtually all the organisms cross the shelf in a narrow pulse. A small number of swimmers are delayed through interaction with the westward portion of the eddy, where the currents are offshore. Most of these delayed organisms will eventually cross the shelf via a process that is nicely illustrated by a pathway corresponding to the stable and unstable manifolds of a hyperbolic region to the west of the eddy center.

The dominance of swimming, as opposed to eddy advection, for directional onshore swimming at speeds more than about 1 cm s^{-1} brings into question the overall importance of the eddy for all but passively advected or very slow organisms. Indeed, Wuenschel and Able (2008) observed that glass eels can swim short-term at speeds up to 12 cm s^{-1} . However, their navigation ability is unknown. The ability to maintain a given direction and navigate directly onshore, either by hearing the sounds coming from the shelf, or by detecting gradients in ocean water salinity, or navigating by Earth's magnetic field, has a major influence on the success rate of the organisms in crossing the shelf break. Organisms, even fast-swimming organisms, which cannot maintain onshore direction, are influenced much more by the oceanic currents than the slow swimmers that navigate directly onshore. Specifically, numerical

simulations with organisms that swim at $V_s = 10 \text{ cm s}^{-1}$ (i.e., fast swimmers) but change direction every minute ($\delta t = 1 \text{ min}$), instead of directly swimming onshore as in all of our other simulations, yield cross-shelf transport similar to that for passive nonswimming organisms (i.e., similar to Fig. 4a). This result is consistent with a statistical prediction; specifically, for a random-walk process with these parameters the root-mean-square distance from the initial position of a random walker grows as $d_{\text{rms}} = V_s \sqrt{\delta t \sqrt{T}}$, reaching only 5 km after 1 year. Because this distance is significantly smaller than the eddy radius, the effects of the random swimming are minor, and the resulting cross-shelf transport for random swimmers is similar to that for passively advected particles.

Acknowledgments. IR and LP were supported by National Science Foundation (NSF) Grant OCE-1558806. DC was supported by NSF U.S. National Science Foundation's Physical Oceanography program through Grants OCE-1059632 and OCE-1433953 as well as the Academic Programs Office, Woods Hole Oceanographic Institution. We acknowledge high-performance computing support from Yellowstone (<http://n2t.net/ark:/85065/d7wd3xhc>) provided by NCAR's Computational and Information Systems Laboratory, sponsored by the National Science Foundation.

REFERENCES

- Brink, K. H., 1998: Deep sea forcing and exchange processes. *The Global Coastal Ocean: Processes and Methods*, K. H. Brink and A. R. Robinson, Eds., Vol. 10, *The Sea—Ideas and Observations on Progress in the Study of the Seas*, John Wiley and Sons, 151–167.
- , 2016: Cross-shelf exchange. *Annu. Rev. Mar. Sci.*, **8**, 59–78, <https://doi.org/10.1146/annurev-marine-010814-015717>.
- Cherian, D. A., and K. H. Brink, 2016: Offshore transport of shelf water by deep-ocean eddies. *J. Phys. Oceanogr.*, **46**, 3599–3621, <https://doi.org/10.1175/JPO-D-16-0085.1>.
- , and —, 2018: Shelf flows forced by deep-ocean anticyclonic eddies at the shelf break. *J. Phys. Oceanogr.*, **48**, 1117–1138, <https://doi.org/10.1175/JPO-D-17-0237.1>.
- Frolov, S. A., G. G. Sutyrin, G. D. Rowe, and L. M. Rothstein, 2004: Loop Current eddy interaction with the western boundary in the Gulf of Mexico. *J. Phys. Oceanogr.*, **34**, 2223–2237, [https://doi.org/10.1175/1520-0485\(2004\)034<2223:LCEIWT>2.0.CO;2](https://doi.org/10.1175/1520-0485(2004)034<2223:LCEIWT>2.0.CO;2).
- Garfield, N., III, and D. L. Sutyrin, 1987: Shelf water entrainment by Gulf Stream warm-core rings. *J. Geophys. Res.*, **92**, 13 003–13 012, <https://doi.org/10.1029/JC092iC12p13003>.
- Haller, G., 2002: Lagrangian coherent structures from approximate velocity data. *Phys. Fluids*, **14**, 1851–1861, <https://doi.org/10.1063/1.1477449>.
- , 2011: A variational theory of hyperbolic Lagrangian coherent structures. *Physica D*, **240**, 574–598, <https://doi.org/10.1016/j.physd.2010.11.010>.
- , 2015: Lagrangian coherent structures. *Annu. Rev. Fluid Mech.*, **47**, 137–162, <https://doi.org/10.1146/annurevfluid-010313-141322>.

- Hare, J. A., and R. K. Cowen, 1996: Transport mechanisms of larval and pelagic juvenile bluefish (*Pomatomus saltatrix*) from South Atlantic Bight spawning grounds to Middle Atlantic Bight nursery habitats. *Limnol. Oceanogr.*, **41**, 1264–1280, <https://doi.org/10.4319/lo.1996.41.6.1264>.
- , and Coauthors, 2002: Routes and rates of larval fish transport from the southeast to the northeast United States continental shelf. *Limnol. Oceanogr.*, **47**, 1774–1789, <https://doi.org/10.4319/lo.2002.47.6.1774>.
- Joyce, T. M., J. K. Bishop, and O. B. Brown, 1992: Observations of offshore shelf-water transport induced by a warm-core ring. *Deep-Sea Res.*, **39A**, S97–S113, [https://doi.org/10.1016/S0198-0149\(11\)80007-5](https://doi.org/10.1016/S0198-0149(11)80007-5).
- Lee, C. M., and K. H. Brink, 2010: Observations of storm-induced mixing and Gulf Stream ring incursion over the southern flank of Georges Bank: Winter and summer 1997. *J. Geophys. Res.*, **115**, C08008, <https://doi.org/10.1029/2009JC005706>.
- Lee, T. N., M. E. Clarke, E. Williams, A. F. Szmant, and T. Berger, 1994: Evolution of the tortugas gyre and its influence on recruitment in the Florida keys. *Bull. Mar. Sci.*, **54**, 621–646.
- Lekien, F., and S. D. Ross, 2010: The computation of finite-time Lyapunov exponents on unstructured meshes and for non-Euclidean manifolds. *Chaos*, **20**, 017505, <https://doi.org/10.1063/1.3278516>.
- Lentz, S. J., 2010: The mean along-isobath heat and salt balances over the Middle Atlantic Bight continental shelf. *J. Phys. Oceanogr.*, **40**, 934–948, <https://doi.org/10.1175/2009JPO4214.1>.
- Limouzy-Paris, C. B., H. C. Graber, D. L. Jones, A. W. Röpke, and W. J. Richards, 1997: Translocation of larval coral reef fishes via sub-mesoscale spin-off eddies from the Florida Current. *Bull. Mar. Sci.*, **60**, 966–983.
- McWilliams, J. C., and G. R. Flierl, 1979: On the evolution of isolated, nonlinear vortices. *J. Phys. Oceanogr.*, **9**, 1155–1182, [https://doi.org/10.1175/1520-0485\(1979\)009<1155:OTEIOIN>2.0.CO;2](https://doi.org/10.1175/1520-0485(1979)009<1155:OTEIOIN>2.0.CO;2).
- Oey, L.-Y., and H. Zhang, 2004: The generation of subsurface cyclones and jets through eddy-slope interactions. *Cont. Shelf Res.*, **24**, 2109–2131, <https://doi.org/10.1016/j.csr.2004.07.007>.
- Okkonen, S. R., T. J. Weingartner, S. Danielson, D. Musgrave, and G. Schmidt, 2003: Satellite and hydrographic observations of eddy-induced shelf-slope exchange in the northwestern Gulf of Alaska. *J. Geophys. Res.*, **108**, 3033, <https://doi.org/10.1029/2002JC001342>.
- Olascoaga, M. J., I. I. Rypina, M. G. Brown, F. J. Beron-Vera, H. Kocak, L. E. Brand, G. R. Halliwell, and L. K. Shay, 2006: Persistent transport barrier on the west Florida shelf. *Geophys. Res. Lett.*, **33**, L22603, <https://doi.org/10.1029/2006GL027800>.
- Olson, D. B., 1991: Rings in the ocean. *Annu. Rev. Earth Planet. Sci.*, **19**, 283–311, <https://doi.org/10.1146/annurev.earth.19.050191.001435>.
- Ramp, S. R., R. C. Beardsley, and R. Legeckis, 1983: An observation of frontal wave development on a shelf-slope/warm core ring front near the shelf break south of New England. *J. Phys. Oceanogr.*, **13**, 907–912, [https://doi.org/10.1175/1520-0485\(1983\)013<3C0907:AOFWD%3E2.0.CO;2](https://doi.org/10.1175/1520-0485(1983)013<3C0907:AOFWD%3E2.0.CO;2).
- Richardson, D. E., and R. K. Cowen, 2004: Diversity of leptocephalus larvae around the island of Barbados (West Indies): Relevance to regional distributions. *Mar. Ecol. Prog. Ser.*, **282**, 271–284, <https://doi.org/10.3354/meps282271>.
- Rypina, I. I., M. G. Brown, and H. Kocak, 2009: Transport in an idealized three-gyre system with application to the Adriatic Sea. *J. Phys. Oceanogr.*, **39**, 675–690, <https://doi.org/10.1175/2008JPO3975.1>.
- , L. J. Pratt, J. Pullen, J. Levin, and A. Gordon, 2010: Chaotic advection in an archipelago. *J. Phys. Oceanogr.*, **40**, 1988–2006, <https://doi.org/10.1175/2010JPO4336.1>.
- , J. K. Llopiz, L. J. Pratt, and M. S. Lozier, 2014: Dispersal pathways of American eel larvae from the Sargasso Sea. *Limnol. Oceanogr.*, **59**, 1704–1714, <https://doi.org/10.4319/lo.2014.59.5.1704>.
- , L. J. Pratt, and M. S. Lozier, 2016: Influence of ocean circulation changes on the inter-annual variability of American eel larval dispersal. *Limnol. Oceanogr.*, **61**, 1574–1588, <https://doi.org/10.1002/lno.10297>.
- Shchepetkin, A. F., and J. C. McWilliams, 2005: The Regional Oceanic Modeling System (ROMS): A split-explicit, free-surface, topography - following coordinate oceanic model. *Ocean Modell.*, **9**, 347–404, <https://doi.org/10.1016/j.ocemod.2004.08.002>.
- Shi, C., and D. Nof, 1993: The splitting of eddies along boundaries. *J. Mar. Res.*, **51**, 771–795, <https://doi.org/10.1357/0022240933223927>.
- Sponaugle, S., T. Lee, V. Kourafalou, and D. Pinkard, 2005: Florida Current frontal eddies and the settlement of coral reef fishes. *Limnol. Oceanogr.*, **50**, 1033–1048, <https://doi.org/10.4319/lo.2005.50.4.1033>.
- Stewart, A. L., and A. F. Thompson, 2015: Eddy-mediated transport of warm Circumpolar Deep Water across the Antarctic shelf break. *Geophys. Res. Lett.*, **42**, 432–440, <https://doi.org/10.1002/2014GL062281>.
- Tesch, F. W., 1980: Occurrence of eel *Anguilla anguilla* larvae west of the European continental shelf, 1974–1977. *Environ. Biol. Fishes*, **5**, 185–190, <https://doi.org/10.1007/BF00005354>.
- , U. Niermann, and A. Plaga, 1986: Differences in development stage and stock density of larval *Anguilla anguilla* off the west coast of Europe. *Vie Milieu*, **36**, 255–260.
- , J. Thorpe, and R. J. White, 2003: *The Eel*. Blackwell Publishing, 416 pp.
- Tranter, D. J., D. J. Carpenter, and G. S. Leech, 1986: The coastal enrichment effect of the East Australian current eddy field. *Deep-Sea Res.*, **33A**, 1705–1728, [https://doi.org/10.1016/0198-0149\(86\)90075-0](https://doi.org/10.1016/0198-0149(86)90075-0).
- Tur, A., and V. Yanovsky, 2017: *Coherent Vortex Structures in Fluids and Plasmas*. Springer, 306 pp.
- Vukovich, F. M., and E. Waddell, 1991: Interaction of a warm ring with the western slope in the Gulf of Mexico. *J. Phys. Oceanogr.*, **21**, 1062–1074, [https://doi.org/10.1175/1520-0485\(1991\)021%3C1062:IOAWRW%3E2.0.CO;2](https://doi.org/10.1175/1520-0485(1991)021%3C1062:IOAWRW%3E2.0.CO;2).
- Wei, J., and D.-P. Wang, 2009: A three-dimensional model study of warm core ring interaction with continental shelf and slope. *Cont. Shelf Res.*, **29**, 1635–1642, <https://doi.org/10.1016/j.csr.2009.05.009>.
- , —, and C. N. Flagg, 2008: Mapping Gulf Stream warm core rings from shipboard ADCP transects of the Oleander Project. *J. Geophys. Res.*, **113**, C10021, <https://doi.org/10.1029/2007JC004694>.
- Wuenschel, M., and K. Able, 2008: Swimming ability of eels (*Anguilla rostrata*, *Conger oceanicus*) at estuarine ingress: Contrasting patterns of cross-shelf transport? *Mar. Biol.*, **154**, 775–786, <https://doi.org/10.1007/s00227-008-0970-7>.
- Zhang, W. G., and G. G. Gawarkiewicz, 2015: Dynamics of the direct intrusion of Gulf Stream ring water onto the Mid-Atlantic Bight shelf. *Geophys. Res. Lett.*, **42**, 7687–7695, <https://doi.org/10.1002/2015GL065530>.